*Journal of Sound and Vibration* (1997) **208**(5), 777–801

# THE AEROACOUSTICS AND AERODYNAMICS OF HIGH-SPEED COANDA DEVICES, PART 1: CONVENTIONAL ARRANGEMENT OF EXIT NOZZLE AND SURFACE

P. W. CARPENTER

*Department of Engineering, University of Warwick, Coventry CV4 7AL, England*

AND

P. N. GREEN

*Department of Computation, UMIST, PO Box 88, Manchester M60 1QD*

(*Received* 23 *January* 1996, *and in final form* 14 *July* 1997)

The literature on high-speed Coanda flows and its applications is reviewed. The lack of basic information for design engineers is noted. The present paper is based on an investigation of the aeroacoustics and aerodynamics of the high-speed Coanda flow that is formed when a supersonic jet issues from a radial nozzle and adheres to a tulip-shaped body of revolution. Schlieren and other flow visualization techniques together with theoretical methods are used to reveal the various features of this complex flow field. The acoustic characteristics were obtained from measurements with an array of microphones in an anechoic chamber. The emphasis is placed on those features of the aerodynamics and aeroacoustics which may be of general interest.

© 1997 Academic Press Limited

## 1. INTRODUCTION

Few readers can have avoided the occasional melancholy experience of attempting to pour a liquid from a badly designed teapot or jug into a cup, only to find that some of the liquid flows around the spout, thereby missing the target. Observing the deflection of a slowly flowing water jet by a judiciously placed finger is another related, but less irritating, everyday experience. These common phenomena are both examples of the tendency of a fluid jet to adhere to an adjoining solid surface. Such phenomena are usually grouped together under the general term *Coanda* effect. The name derives from the Romanian engineer, Henri Coanda [1] who filed a French patent in 1932 for a propulsive device exploiting the phenomenon. In fact, the first relevant scientific observations were probably made by Thomas Young in 1800 [2] (cited on p. 157 of reference [3]). Unlike the simple examples described above the present paper is concerned with Coanda devices operating with high-speed gas flow. There are many examples of such devices in use in industry, some of which will be briefly described below.

The tendency of a fluid jet issuing tangentially to a curved surface to adhere to it as illustrated in Figure 1(a)—is often regarded solely as an inviscid effect. In fact, many of the early theoretical papers (see the review by Wille and Fernholz [4]) were based on potential theory. It is, indeed, easy to see that the radial equilibrium of the fluid element depicted in Figure 1(a) dictates that a pressure field be set up which forces the fluid against the surface. But this does not explain why the equally valid solution shown in Figure 1(b)

0022–460X/97/500777 + 25 $25.00/0/sv971202 © 1997 Academic Press Limited

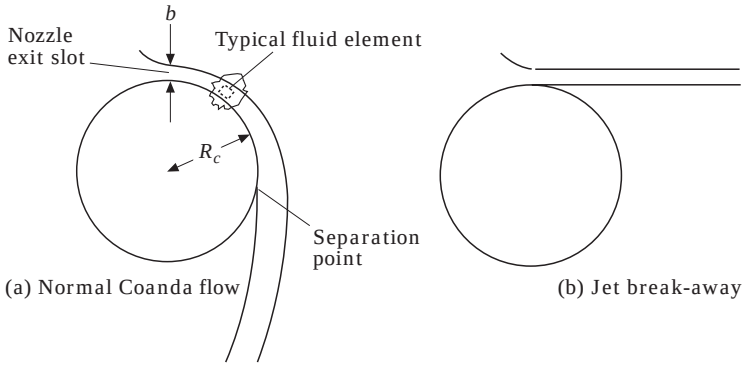


Figure 1. Flow of a jet around a circular cylinder.

is only found in practice when the Coanda effect breaks down. Presumably the slightly enhanced viscous drag experienced by the jet on the surface side as it emerges from the nozzle tends to deflect it towards the surface. Thereafter the pressure field set up by the requirements of radial equilibrium will tend to force the jet towards the surface. Another viscous effect, namely entrainment of the fluid between the jet and the surface, also may help to move the jet towards the surface.

A characteristic of Coanda flows, that is exploited in some applications, is the enhanced turbulence levels and entrainment compared with those of round jets. This characteristic can be attributed to the additional rate of strain associated with convex streamline curvature (see reference [5]). It can also be understood from the standpoint of flow stability. The outer part of the laminar wall layer over a convexly curved surface is susceptible to centrifugal instability. Accordingly one can anticipate that much the same mechanism that is responsible for the formation of Görtler vortices in boundary layers over concave surfaces will give rise to coherent structures in the form of streamwise vortices in the outer part of the curved wall jet. For axisymmetric Coanda flows the entrainment and turbulence levels are enhanced still further by flow divergence (see reference [5, 6]). Coanda flows are also often found to be quieter and more stable (in a global sense) than conventional alternatives. For example, this has been commented on by Wilkins *et al*. [7], Desty *et al*. [8] and Fricker *et al*. [9].

Probably the most extensively studied application of high-speed Coanda flows is to be found in circulation-control (CC) aerofoils and wings. A high-speed air jet issues tangentially over a rounded trailing edge or flap and, owing to the Coanda effect, the flow over the trailing edge is deflected downwards leading to greatly enhanced circulation and lift coefficients, several times greater than those found with conventional aerofoils. It appears that the concept originated in the UK with Cheeseman and Seed [10], but subsequent development has been carried out mainly in the USA. Several papers on CC wings are to be found in reference [11] and overviews of steady and unsteady CC respectively have been given by Wood and Nielsen [12] and Zandieh and Leishman [13]. Two aeronautical applications of the Coanda effect related to CC are upper-surface blowing (see references [14, 15]) and thrust vectoring (see reference [16, 17]). High-speed jet flows are involved in both cases.

Most of the non-aeronautical industrial applications of high-speed Coanda flow exploit the enhanced entrainment characteristics. Probably the most widely used device is the Coanda jet pump whereby a high-speed primary flow issues from a slot and adheres to the wall of a convergent–divergent nozzle. The enhanced entrainment due to the primary jets induces a secondary flow into the nozzle in much the same way as for a conventional

jet jump or ejector. According to Desty [18]: "Units... with capacities ranging from a few cubic feet per minute to tens of thousands of cubic feet per minute are now well established particularly for ventilation purposes in hazardous environments like coal mines". Despite the Coanda jet pump's widespread use, however, according to Ameri and Dybbs [19, 20] there appears to be little information about its design in the open literature.

Various burners and combusters also exploit the enhanced entrainment and turbulence levels found in high-speed Coanda flows. Desty *et al*. [7, 8, 18] described the operation of the Mardair waste-gas flare and Fricker *et al*. [9] described a burner used by British Gas. Both devices are essentially jet-pump burners, i.e., internal Coanda devices. Desty *et al*. [7, 8, 18, 21] also described two types of external Coanda waste-gas flares: the Indair, which has an axisymmetric tulip-shaped Coanda surface (see Figures 2–4), and the Stedair, a steam-assisted flare. The maximum diameter of the full-sized Indair can range from 33 to 108 in and the operating pressure can exceed 5 bar. Desty [18] claimed in 1983 that the 108 in Indair produced the largest man-made flame yet created. The Indair is of particular significance here, because the present work was carried out as part of a research programme on its aeroacoustics and aerodynamics.

Owing to the somewhat miscellaneous nature of the applications a substantial methodical body of literature on Coanda flow has not really been developed, possibly leaving design engineers at a loss. The CC wing is, perhaps, the exception to this rule. The sort of general information required by design engineers is as follows.

(i) *Separation and breakdown characteristics*. For reasons that will be more fully explained in section 3, the Coanda flow around a circular cylinder (and, by analogy, other curved surfaces) will eventually separate. When parameters, such as operating pressure, nozzle-exit slot width and curvature are increased the separation point retreats around the surface back towards the nozzle exit. At some critical point the flow breaks away completely from the surface as shown in Figure 1(b). At high speeds the separation

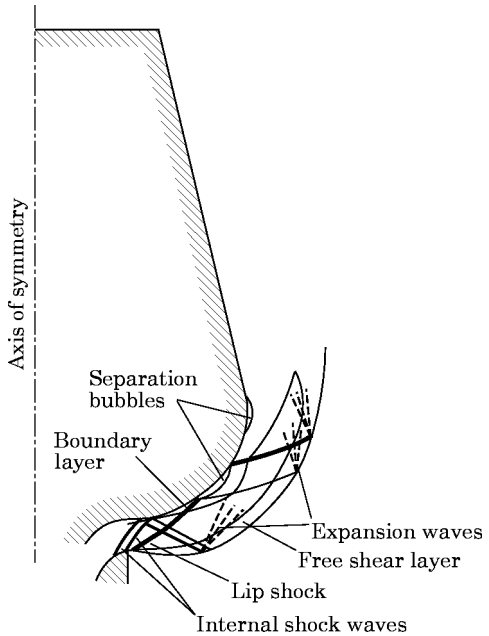


Figure 2. Schematic diagram of the key features of the flow field for a model Indair flow. (Note that the nozzle-exit width is greatly exaggerated.)

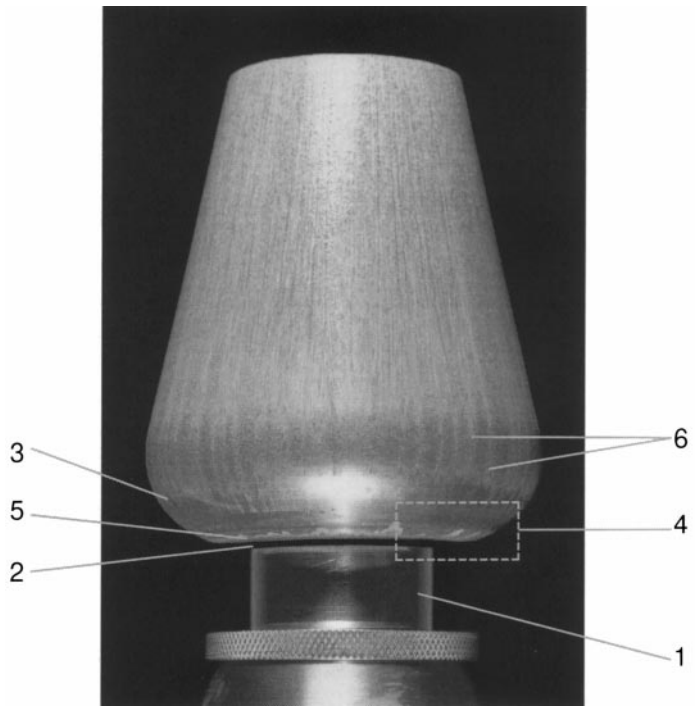


Figure 3. A photograph of the Coanda model with exit slot width adjusted to configuration C of Table 1. The figure also shows a surface oil-film flow visualization carried out at a stagnation pressure ratio $p_0/p_\infty = 5{\cdot}2$. Key: 1, adjustable sleeve for varying slot width; 2, annular exit slot; 3, Coanda surface; 4, region corresponding to schlieren photographs in Figure 6; 5, indications of a separation bubble; and 6, indications of streamwise vortices.

phenomena are further complicated by the occurrence of shockwave/boundary layer interaction.

(ii) *Entrainment and turbulence levels*. The enhanced entrainment and turbulence characteristics of Coanda flows are exploited by many of the applications briefly discussed above. Design engineers need to know how these quantities vary with the operational and geometrical parameters.

(iii) *Acoustic characteristics*. The reduced noise emission associated with Coanda flows is often another reason for choosing a Coanda device; see, for example, references [8, 9, 21]. Accordingly it is important that design engineers have access to suitable information on the acoustic characteristics. There is relatively little information available in the open literature about the aeroacoustics of Coanda flows, apart from our own earlier work on the Indair which is reported in references [22–24], some information in reference [9] about jet-pump-type combusters, the Li and Halliwell [25] comparative study of four industrial Coanda nozzles, and the investigation of the aeroacoustics of CC wings with upper-surface blowing by Salikuddin *et al*. [26].

The present paper describes an experimental and theoretical investigation of a particular high-speed Coanda flow. The investigation was fairly comprehensive, but only the features which are considered to be of general interest are presented and discussed here. The remainder of the paper is set out as follows: section 2 describes the experimental set-up; section 3 describes the general features of the flow field; the acoustic characteristics are described in section 4; section 5 is devoted to a particular aspect of the acoustic

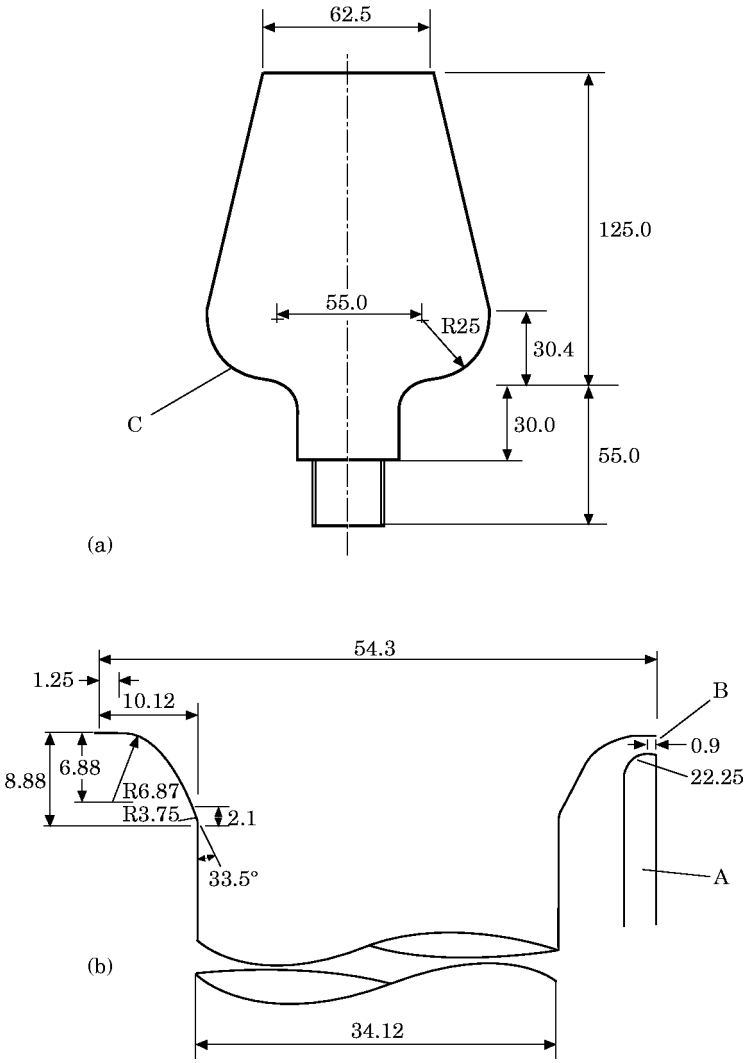


Figure 4. Details of the geometry of the model Indair flare. (a) Model flare tip. (b) Model nozzle geometry. Key: A, adjustable sleeve; B, annular exit slot; and C, Coanda surface.

characteristics, namely shock-associated noise and the generation of discrete tones; and the conclusions follow in section 6.

## 2. THE EXPERIMENTAL STUDY

The experimental investigation of high-speed Coanda flows had two major components, namely a flow-visualisation study and a programme of acoustic measurements. Both sets of experiments made use of the same Coanda model, which is shown in Figures 2–4. Figure 3 also shows a surface oil film flow visualization, but is included at this point to depict the form of the Coanda model. This model is a "tulip-shaped" body of revolution with the exit slot of the annular nozzle located at the base of the tulip. It is, in fact, a 1/8th scale model of a 33 in Indair waste gas flare, designed and marketed by Kaldair Ltd. Usually Indair flares are fitted with a step between the nozzle exit and the Coanda surface,

TABLE 1

*Dimensions of exit slots*

| Slot | Slot-width $b$ (mm) | $b/R_C$ |
|---|---|---|
| A | 0·625 | 0·025 |
| B | 1·25 | 0·05 |
| C | 1·875 | 0·075 |
| D | 2·5 | 0·1 |

which enhances the Coanda effect and ensures that flow breakaway does not occur. The presence of a step, however, makes the flow field and acoustic characteristics rather more complex than the corresponding unstepped case. Accordingly, the step was omitted at this stage of the investigation. The effects of the step on the aeroacoustics will be described in Part 2 of the paper.

The geometry and dimensions of the exterior Coanda surface and interior curved annular nozzle leading to the exit slot are shown in Figure 4. The width of the exit slot is adjustable, and the four different settings shown in Table 1 were used. The third column gives the ratio of the slot width $b$, to the radius $R_C$, of the Coanda surface profile; $R_C = 25$ mm for the present model.

High-pressure air was used as the working fluid and supplied at a controlled stagnation pressure by means of a blow-down facility. The quoted values of stagnation pressure were measured by means of a strain-gauge pressure transducer just upstream of the nozzle exit. The maximum working pressure used was 80 psig (5·52 bar). The corresponding stagnation temperature was also measured.

A comprehensive investigation of the flow field was carried out by means of the schlieren, shadowgraph and oil-film methods. The schlieren study was particularly extensive, with a wide range of slot-width/stagnation-pressure combinations being considered.

Several different sets of schlieren photographs were obtained by varying the configuration of the optical system to highlight features of interest in the flow. The results of the flow visualization study, and calculations performed with the method of characteristics form the basis of many of the observations made in section 3 concerning the flow field. Further details of the experimental set-up and techniques have been given by Green [27].

The acoustic measurements were carried out in an anechoic chamber measuring 5 m × 3 m × 5 m, with a vertically mounted model. The general set-up is depicted schematically in Figure 5. The interior walls of the chamber are lined with 50 mm thick acoustic foam which rendered it anechoic in the frequency range of interest (20–80 kHz). A circular-arc array of eight Brüel and Kjaer Type 4135 1/4 in microphones, centred on the exit slot of the model, were used giving a flat frequency response up to 80 kHz. The radius of the arc was 1 m and the microphones were located at −50, −37·5, −25, −12·5, 0, 20, 40 and 60 degrees relative to the horizontal.

The microphone signals were fed via preamplifiers and amplifiers to an eight-channel precision tape recorder. Subsequently the data were transmitted via an analogue-to-digital converter to a mainframe computer where fast Fourier transform techniques were used to process the data. The power spectra were averaged 50 times to obtain adequate statistical reliability. The main reason for using a tape recorder was to allow the effective signal frequencies to be reduced by playing back the tape at a slower speed than used during recording. This was necessary because otherwise the analogue-to-digital converter could

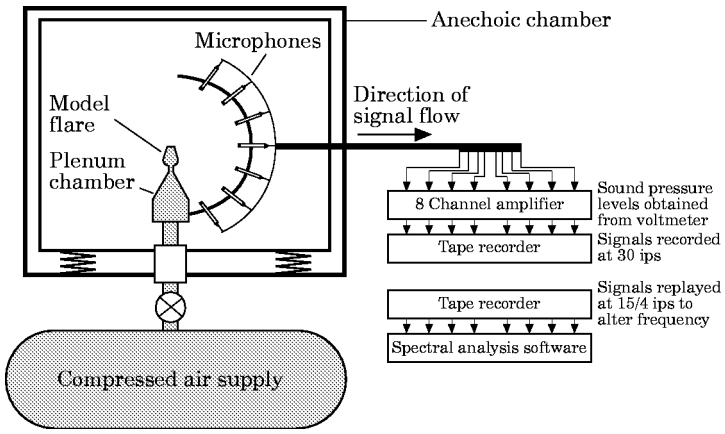


Figure 5. Schematic diagram of the acoustic measurement system.

not sample fast enough to avoid spectral aliasing. Additional details of the acoustic measurements and the signal processing techniques can be found in reference [27].

## 3. FEATURES OF THE FLOW FIELD

Essentially the flow field under consideration is formed when a high-speed gas jet issues from a radial nozzle located at the base of a tulip-shaped body of revolution to which it adheres thereby forming a wall jet. A schematic sketch showing the principal features of the flowfield is given in Figure 2. Many other significant features that are discussed below are omitted in the interests of clarity. For the same reason the width of the exit slot and consequently that of the wall jet are greatly exaggerated. When the gauge pressure exceeds about 1 bar the flow becomes underexpanded and an increasingly complex pattern of shock waves form as the operating pressure (i.e., nozzle stagnation pressure) rises. An extensive flow-visualization investigation of the flow field has been carried out, by means of schlieren, shadowgraph and surface-film techniques. Various theoretical studies have also been undertaken to complement the experimental investigations. Typical surface-flow visualizations and spark schlieren photographs for high operating pressures are displayed in Figures 3 and 6 respectively. The region of the flow field corresponding to the schlieren photographs is indicated by the broken white lines labelled 4 in Figure 3. The detailed features of the flow field are, of course, dictated by the geometrical design of the nozzle and Coanda surface. Full details and a comprehensive set of results can be found in reference [27]. Here the authors focus on the key features of this highly complex flow field which are likely to be found in other high-speed Coanda flows. For example, although it should be obvious to aerodynamicists, it is often not realized by non-specialists that shock waves will inevitably be present in high-speed Coanda flows. This was not initially appreciated when the Coanda-type waste gas flares were developed. For small Coanda devices the exit slot is often so minute that the shock waves present near the nozzle exit can easily be overlooked in schlieren photographs of the whole flow field. This was probably true for the Coanda devices studied by Li and Halliwell [25].

### 3.1. TURBULENT SHEAR LAYERS

In many respects the turbulent shear layers develop in a similar way as for a conventional jet. A free shear layer (see label 8 in Figure 6) grows around the outer jet boundary near

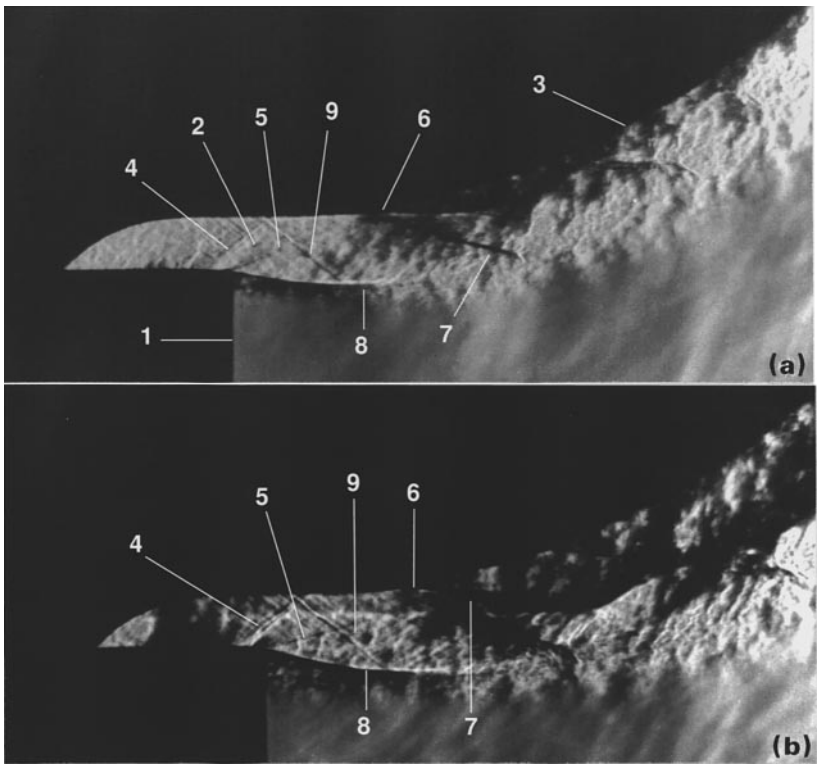


Figure 6. Spark schlieren photographs of the flow field corresponding to the region 4 in Figure 3 near the nozzle exit for slot C. (a) Pressure ratio, $p_0/p_\infty = 4{\cdot}79$; (b) $p_0/p_\infty = 5{\cdot}83$. Key: 1, adjustable sleeve; 2, fan of expansion waves; 3, Coanda surface; 4, internal shock wave; 5, lip shock; 6, leading edge of separation bubble; 7, separation shock wave; 8, edge of jet; 9, reflected shock wave.

the exit slot and a thin boundary layer forms on the surface. At about two or three slot widths downstream of the exit slot the free shear layer and boundary layer merge and a fully developed wall layer begins. A theoretical study of the mixing layer has been carried out in references [6, 27]. Since the turbulent flow in the mixing layer is experiencing additional strain rates due to streamline curvature and radial expansion, the levels of turbulence tend to be considerably higher than the corresponding plane mixing layer and wall jet. On the other hand the actual growth rate of the mixing layer for the Coanda flow is not greatly different from that of the plane mixing layer. Nevertheless the "potential core" tends to be shorter because, owing to radial expansion, the inviscid jet boundary moves towards the surface in order to conserve mass flow. Calculations and measurements of the wall jet emanating from a tangential slot nozzle and developing over a circular cylinder have been presented by Newman [28] and Morrison and Gregory-Smith [29]. The latter and Gregory-Smith and Hawkins [30] have also carried out such studies for the flow field of the Indair-type Coanda flare.

### 3.2. FLOW SEPARATION AND BREAK-AWAY

Coanda flows will inevitably separate from the surface at some point, as shown in Figure 1(a). This can be explained by considering the radial equilibrium of the fluid element depicted in Figure 1(a) which can be expressed as

$$\partial p/\partial r = \rho V^2/r, \tag{1}$$

where $p$ is the pressure within the shear layer, $r$ is the radial distance from the centre of curvature, $\rho$ is the fluid density and $V$ is the local flow speed. Upon assuming initially that the flow is inviscid it follows from the Bernoulli equation that

$$p = p_0 - \tfrac{1}{2}\rho V^2, \tag{2}$$

where $p_0$ is the stagnational pressure. The pressure can then be eliminated between equations (1) and (2) to give

$$\mathrm{d}V/V = \mathrm{d}r; \qquad \text{i.e.,} \qquad V = V_w \exp(-r/R_c), \tag{3}$$

where $V_w$ is the (inviscid) flow speed along the wall and $R_c$ is the radius of curvature of the surface. When the ratio of exit-slot width to radius of curvature is small $r \simeq R_c$ and $V \simeq V_w$ and it follows from equation (1) that near the exit slot the pressure at the wall is given by

$$p_w = p_\infty - \rho V^2 b/R_c, \tag{4}$$

where $p_\infty$ is the ambient pressure.

It can be seen from equation (4) that the larger $\rho V^2 b/R_c$ is, the more the wall pressure falls below the ambient level. In an actual viscous flow the average flow speed tends to fall with distance around the surface. Consequently the wall pressure rises with distance around the surface leading to an adverse pressure gradient and eventual separation. Newman [28] found empirically that, for fixed $R_c$ and small values of $b/R_c$ at least, the separation point depended only on the parameter

$$\Pi = (p_0 - p_\infty) b R_c / \rho v^2, \tag{5}$$

where $v$ is the kinematic viscosity of the fluid. When $\Pi \geqslant 1{\cdot}6 \times 10^9$ the separation point remains constant at about 245°. The separation point retreats back towards the nozzle exit for smaller values of $\Pi$.

At a sufficiently small value of $\Pi$ the flow will break away completely from the surface, as shown schematically in Figure 1(b). If it is assumed that this happens at a particular value of $\Pi$ then for fixed $p_\infty$ and $R_c$ the break-away pressure ratio follows the trend given below:

$$(p_0/p_\infty - 1) \propto R_c/b. \tag{6}$$

The experimental results of Sokolova [31] and Gregory-Smith and Gilchrist [32] broadly follow this trend, even though the exit flows were supersonic. For high-speed flow, of course, shock wave/boundary layer interaction and other compressible flow effects will complicate matters. Bradbury and Wood [33] found that the separation point moved nearer to the nozzle as the Mach number rises. Sokolova [31] found that for supersonic Coanda flow the separation angle fell steeply as $b/R$ was increased for a convergent–divergent nozzle whereas it did not change much for a convergent nozzle. In both cases, though, she found that a small change in $p_0$ could lead to a rapid fall in the separation angle with subsequent breakaway. This behaviour was also observed by Gregory-Smith and Gilchrist [32] and ourselves. Physically what appears to happen is that shock wave/boundary layer interaction causes separation bubbles to form (see labels 5 in Figures 3 and 6 in Figure 6). These lengthen as $p_0/p_\infty$ rises and the shock waves intensify, until just before breakaway the first separation bubble grows rapidly, ultimately preventing reattachment taking place. This process can be seen by comparing Figures 6(a) and (b). The latter shows the flow near the exit nozzle at a pressure ratio just below the critical break-away value.

Another feature of high-speed Coanda flows is revealed when the stagnation pressure is raised until breakaway occurs, and then reduced to make the flow reattach. It is found that the pressure has to be reduced to a considerably lower value than the breakaway pressure before reattachment occurs. This sort of hysteresis effect was noted in references [16, 24, 32]. The authors have found that for a substantial range of stagnation pressures there appears to be two or more stable states. Simultaneous schlieren, surface visualization and acoustic measurements revealed that abrupt changes in the flow and sound field can occur when the stagnation pressure is changed slightly within this range. In some cases the flow lost its axial symmetry, taking up different flow configurations on adjacent portions of the Coanda surface.

### 3.3. MACH AND SHOCK WAVE SYSTEMS

Many of the flowfield features can be interpreted as resulting from the superposition of two systems of waves. Firstly there is the system of expansion and compression/shock waves normally associated with under-expanding jets. Under-expansion is the cause of the swelling of the jet boundary depicted in Figure 2 and evident in the schlieren photographs of Figure 6. The system of expansion and compression waves is also clearly shown in the computed flow field, presented in Figure 7 which was obtained by using the method of characteristics. A fan of expansion waves emanates from the nozzle lip (see label 2 in Figure 6a). These reflect from the curved surface as expansion waves and then reflect from the jet boundary as compression waves. The latter tend to coalesce into shock waves, at which point the computation was stopped. Thus under-expansion is one mechanism whereby a quasi-periodic system of shock-waves could be generated. In cases where the under-expansion is fairly severe (i.e., $p_0/p_\infty$ is fairly large) a lip shock also forms at the nozzle exit. This too is shown in Figure 2 and is evident in the schlieren photographs (see label 5 in Figure 6).

A second system of Mach waves is also present. These are generated by the radial expansion of the flow and appear in Figure 7 as the downward running lines originating at the nozzle exit. (In contrast, for plane or round free jets uniform flow would exist upstream of the leading expansion wave emanating from the nozzle lip.) This second set of Mach waves reflects from the jet boundary as compression waves and this is thought to be responsible for the diffuse dark regions which appear about one slot width downstream from the nozzle exit in Figure 6(a).

At moderate pressure ratios the calculations carried out by using the method of characteristics correspond fairly well with some of the features revealed by the schlieren photographs. Our calculation method cannot cope with separation bubbles, but Gilchrist and Gregory-Smith [34] have developed a method whereby the method of characteristics

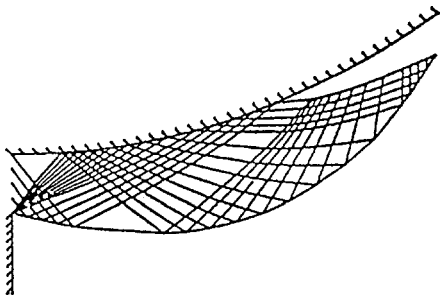

Figure 7. The flow field near the nozzle exit for slot C calculated by using the method of characteristics for a pressure ratio $p_0/p_\infty = 5{\cdot}14$.

can be extended into regions with separation bubbles, provided the location of the separation bubble is specified. They obtained reasonably good correspondence between their calculated flow fields and schlieren photographs, although their work was restricted to the less complex two-dimensional flow with a Coanda similar in profile to that used by us.

### 3.4. SHOCK WAVES EMANATING FROM THE NOZZLE INTERIOR

In Figure 2 a pair of shock waves is shown originating from the lower surface of the nozzle just upstream of the exit. These also show up in the schlieren photographs of Figure 6 (see label 4). It is actually almost impossible to set the knife-edge orientation and exposure in such a way as to obtain one schlieren photograph that show all the details of the nozzle flow as well as the flow field near the nozzle exit and further round the surface. Figure 6 represents a good compromise, but the flow within the nozzle, particularly the features associated with this pair of shock waves, is better shown with a somewhat different set-up of the schlieren system and camera. Based on such studies we have made the sketch shown in Figure 8. It will be noted that a separation bubble is shown as forming on the lower surface of the nozzle.

The features depicted in Figure 8 may, at first sight, seem to be a result of bad nozzle design. In fact, as one demonstrates below, they are an almost inevitable consequence of changing the sign of the streamline curvature. The significance of these curvature-induced shock waves has not, apparently, been previously appreciated, but they are quite evident in many previous papers (see, for example, references [16, 24, 32, 34]). The authors have also seen evidence of similar features in several different industrial applications.

In order to appreciate why these shock waves are generated by changes in the streamline curvature it is helpful to consider how conventional quasi-one-dimensional inviscid nozzle theory could be extended to compressible flow in the sort of curved annular nozzle shown schematically in Figure 9 which is used for the present work. One would first need to choose a suitable local co-ordinate system. This is obtained by calculating the nozzle center-line shown in Figure 9 and then drawing a line perpendicular to it which intersects the nozzle profile. The co-ordinates $s$ along the nozzle centre-line and $n$ along its perpendicular form an orthogonal co-ordinate system which can be used to formulate a quasi-one-dimensional theory. Strictly, because in general the perpendicular distances from the centre-line to each wall of the nozzle are not quite equal, the streamwise

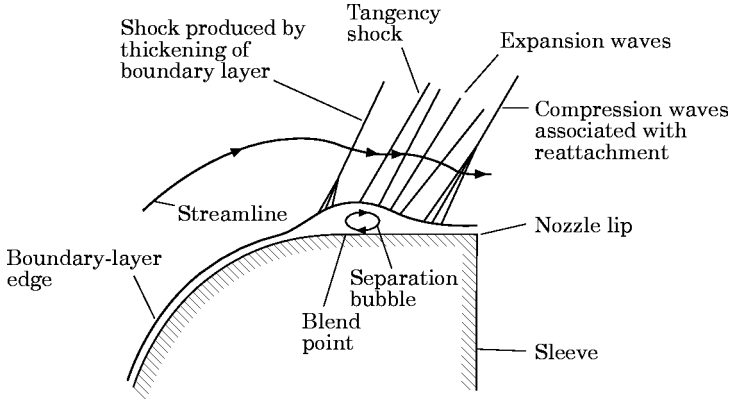


Figure 8. The proposed mechanism for generating shock waves in the nozzle near exit.

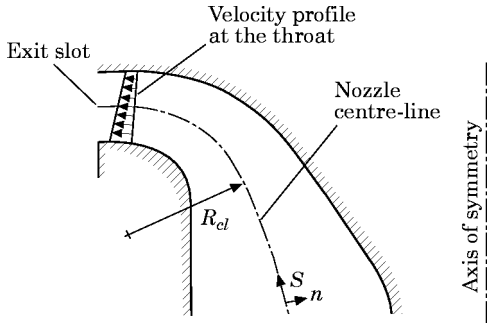


Figure 9. Nozzle geometry and notation. (Note that the orientation differs from Figure 2 in that the nozzle exit is shown on the left.)

co-ordinate should be slightly offset from the center-line in order to make the perpendicular distances to both nozzle walls equal. This refinement is of little consequence to the discussion below.

For present purposes it is not necessary to develop the theory much further, one can simply note that equation (1) still holds for compressible flow and that the isentropic flow relations can be used in place of equation (2) to obtain a minor variation of equation (3) for the local velocity profile,

$$V(s, n) = V(s, 0) \exp(-n/R_{cl}), \tag{7}$$

where $V(s, n)$ is the velocity component in the direction of the centre-line and $R_{cl}$ is its radius of curvature. Equation (7) shows that, unlike the conventional quasi-one-dimensional theory as applied to straight nozzles, for curved nozzles the local velocity profile is not uniform. Rather, as shown in Figure 9, owing to the streamline curvature the flow is faster on the outer wall than on the inner wall. Now consider what happens if the nozzle suddenly becomes straight or the streamline curvature changes sign; both occur in the present case as the flow approaches the nozzle exit and issues out over the Coanda surface. According to equation (7), when this happens the flow on the inner surface is instantaneously accelerated while that on the outer nozzle surface falls abruptly. In practice, of course, the velocity change is sharp rather than discontinuous. Supersonic flow can usually accept sudden acceleration, but a sharp drop in flow speed inevitably generates a shock wave. Thus, provided the flow has become locally supersonic, any sudden change in curvature will generate a shock wave and probably lead to flow separation.

A full account of the quasi-one-dimensional theory has been given in reference [27], together with other applications and results.

## 4. THE ACOUSTIC CHARACTERISTICS

A fairly comprehensive investigation of the acoustic characteristics was carried out and a full account has been given by Green [27]. Here one concentrates only on those aspects of the acoustic characteristics which are considered to be of general interest.

### 4.1. SOUND PRESSURE LEVELS

The sound pressure is plotted in Figure 10 as a function of angle relative to the horizontal for slot A at four different stagnation pressures. Figure 5 shows the orientation of the model; negative angles correspond to directions below the horizontal. It will be noted that the direction of maximum *SPL* moves upward as the pressure rises. The

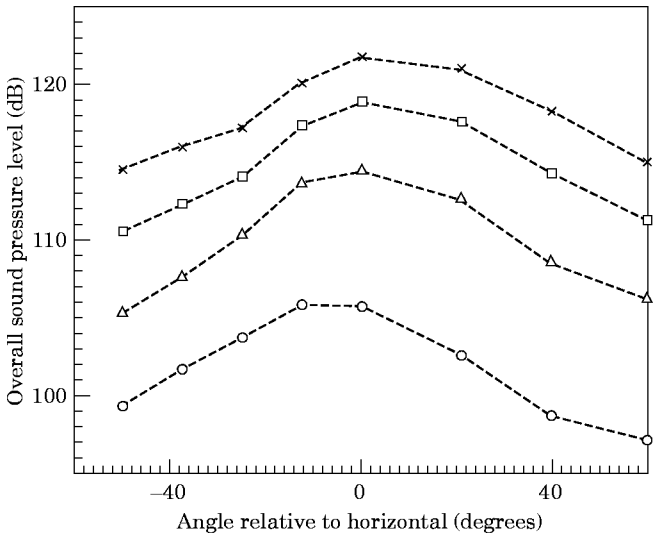


Figure 10. Directivity of overall sound pressure level for slot A. The values of $p_0/p_\infty$ are as follows: ----○----, 2·4; ----△----, 3·8; ----□----, 5·2; ---- × ----, 6·6.

directivity plots for the other exit-slot configurations are not presented, but one can report that for slot B there is a strong departure from the trends of Figure 10 at stagnation pressure ratios of $p_0/p_\infty = 1{\cdot}7$ and 2·0 and for values of this ratio exceeding 3·75 in the case of slots C and D. In all these cases the generation of discrete tones is responsible for the distorted directivity patterns. This will be discussed in section 5.

The variation of the *SPL* radiated in the horizontal direction with the flow speed on the jet boundary at the nozzle exit is plotted in Figure 11 for all four exit slots. The flow speed was calculated from the values of $p_0/p_\infty$ by using isentropic flow relations. Also plotted on Figure 11 is the well-known $U^8$ law due to Lighthill [35] which is followed

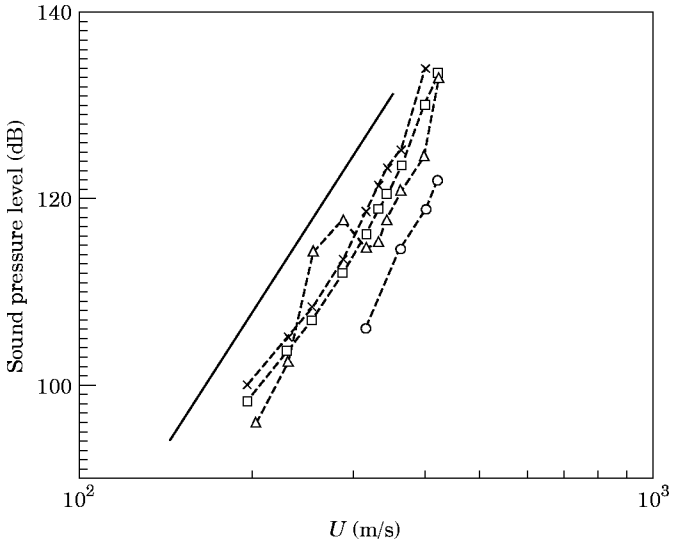


Figure 11. Sound pressure level versus jet boundary velocity for various slot widths. ----○----, slot A; ----△----, slot B; ----□----, slot C; ---- × ----, slot D; ——, $U^8$.

approximately by conventional round jets. Note that the location chosen for the $U^8$ line is arbitrary and only its slope should be compared with the experimental data from the Coanda flow. The data for Slot B depart from the main trend at moderate flow speeds owing to the generation of discrete tones alluded to above. Apart from this there is a fairly close correspondence to the $U^8$ law with some steepening at higher speeds. This steepening is also found for round jets and is usually attributed to convective amplification.

When the effects of the discrete tones are neglected the *SPL* varies roughly with the square of the slot width (i.e., $SPL \propto b^2$). The wall-jet thickness would be expected to be proportional to the slot width, $b$, just as the jet thickness is proportional to the nozzle diameter, $D$, for a round jet. The Lighthill theory predicts that *SPL* is proportional to $D^2$. So the observed variation of *SPL* with $b^2$ for the Coanda flows and the slope of the curves appear to be roughly consistent with Lighthill's theory. But it will be revealed in section 4.2 that not all the experimental observations are consistent with using $b$ as the typical length scale for the classic Lighthill theory.

### 4.2. SPECTRA AND TURBULENCE MIXING NOISE

Some typical *SPL* spectra are shown in Figure 12. In the absence of discrete tones the spectra are broadband in character as illustrated by Figure 12(a). In section 4.1 it appears that the exit-slot width $b$ played a similar role in scaling the acoustic emissions as nozzle diameter does for round jets. Thus it may well be expected that, in analogy with round jets, the broadband peak frequency ($f_p$) would be given by

$$f_p \Lambda / U_c \propto f_p b / U = \text{const} = O(1), \tag{7}$$

where $\Lambda$ and $U_c$ are respectively the length-scale and convection speed characterizing the coherent structures, and $U$ is the flow speed obtained from $p_0/p_\infty$ by using the isentropic flow relations. In fact, the present data show that there is a tendency for the broadband peak frequency to rise with flow speed (or $p_0/p_\infty$), but not as rapidly as it would if it were proportional to flow speed. However, the presence of discrete tones (see Figures 12(b) and (c)) and possibly shock-associated noise (see section 5.2) make it difficult to determine with any confidence the relationship between broadband peak frequency and flow speed. Since for some pressure ratios the discrete tones are absent for all slot widths, it is much easier to discern the variation of peak broadband frequency with exit-slot width.

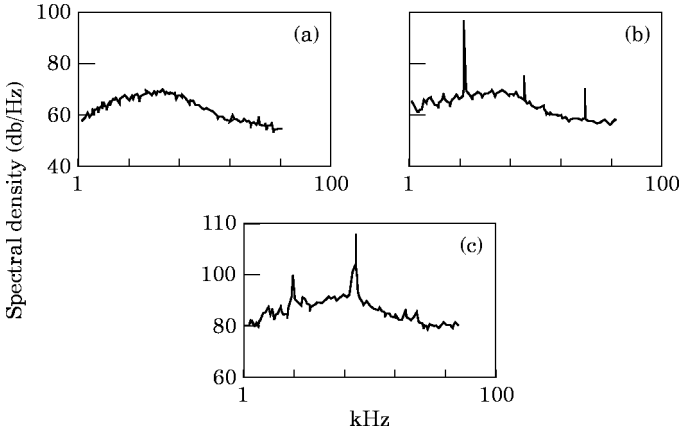


Figure 12. Sound pressure spectra for slot B with observer in the horizontal direction. The values of $p_0/p_\infty$ are as follows: (a) 1·5; (b) 1·7; (c) 6·52.

For directions along or below the horizontal the broadband peak frequency is roughly 40 kHz irrespective of the exit-slot width at a fixed stagnation pressure ratio of 1·5. There is a shift to progressively lower frequencies as the observer angle rises above the horizontal. It is also evident in the data presented by Salikuddin *et al*. [26] for circulation-control wings that peak frequency does not vary appreciably with slot width. So this is possibly a fairly general feature of Coanda flows.

It does appear, however, that the broadband peak frequency $f_p$ increases roughly linearly with the maximum diameter ($D_{max}$) of the tulip-shaped body. This emerged from tests carried out on 8 in and 33 in Indair flares reported by Parsons [36]. A comparison of the spectra from the flares with those from the model used for the present work suggests that the broadband peak frequencies are approximately in the ratio 1:4:8, as would be expected if $f_p \propto D_{max}$. This conclusion should be viewed with some caution, however, since the three spectra were quite different in character. Nevertheless, the limited evidence suggests that the scaling law for peak frequency generated by Coanda flows is approximately

$$f_p D_{max}/U = \text{const.} \tag{8}$$

The authors do not have a good explanation for the marked difference in the peak-frequency scaling laws between the Coanda flow and the round jet. However, there are some differences between the two flows which may be significant. For instance, for the round jet convection effects are absent for observers at right angles to the jet, whereas for the Coanda flow there is no direction for which these effects are absent. Moreover, Smith and Carpenter [37] have shown that for wall jets over plane surfaces the presence of the solid wall intensifies the convection effects. There is also the question of broadband shock-associated noise which will be discussed in section 5.2.

If $b$ and $U$ take the values appropriate to Figure 12(a), i.e., 1·25 mm and 250 m/s, $f_p$ would be of the order of 200 kHz when calculated by using equation (7), rather than around 40 kHz as actually found in Figure 12(a). But this choice of values is based on the assumption that the mixing-layer region, i.e., the turbulent flow near the nozzle exit, contains the dominant noise sources. As remarked above in section 3.1, radial expansion and streamline curvature both promote enhanced turbulence levels and it could be that the main noise-producing regions of the Coanda flow are located a considerable distance round the surface from the exit slot in the vicinity of the maximum diameter where there is also a far greater volume of turbulent flow. At this point the maximum flow speed $U_m$ will be much lower than $U$ (maximum flow speed in the jet just downstream of the exit slot) and the thickness $\delta$ of the wall jet substantially greater than $b$. Substituting the values of $\delta$ and $U_m$ in equation (7) instead of $b$ and $U$ would certainly considerably reduce the estimated value for the peak frequency. When account is taken of the shielding effect of the tulip-shaped body, the variation of peak frequency with direction and the approximate scaling law given in equation (8) are both consistent with the suggestion that the dominant noise sources radiating in the horizontal direction are located near the position of maximum diameter. After all, if the turbulence structures responsible for producing most of the noise are located near this point and take the form of ring vortices extending around the tulip-shaped body, then it would not be surprising if the peak frequency were to scale according to equation (8). Owing to the lack of basic information on the turbulent flow in question it is difficult to support this argument with quantitative estimates, although some attempt is made to do this in reference [27]. In the light of the discussion above one would suggest that in the horizontal direction, at least, turbulent mixing noise is the main source of broadband aerodynamic noise.

## 5. SHOCK-ASSOCIATED NOISE AND THE DISCRETE TONES

A complex pattern of shock waves is present in the Coanda flows for most pressure ratios. Accordingly it is quite likely that shock-associated noise will be generated. This will be discussed below. As is evident from the spectra displayed in Figure 12 discrete tones are generated for certain operating conditions. Actually there are two distinct groups of such tones. Group A appears only at low values of $p_0/p_\infty$ and the dominant frequency is approximately invariant with pressure ratio. Group B appears only at relatively high values of $p_0/p_\infty$ and is characterized by the frequency falling steeply with rising pressure ratio. Group A will be discussed first in section 5.1. An appropriate model for shock-associated noise will then be introduced in section 5.2. This will be followed in sections 5.3 and 5.4 by a discussion of the Group B discrete tones and descriptions of two possible theoretical models of the mechanism responsible for their generation.

### 5.1. GROUP A DISCRETE TONES

The Group A discrete tones were observed solely for exit slot B at pressure ratios from 1·6 to 2·0. According to our quasi-one-dimensional theory (see section 3.4 and reference [27]) the nozzle passage leading to the exit slot is equivalent to a convergent–divergent nozzle (note that the effect of radial expansion can make the appearance of the nozzle profile in Figure 9 somewhat misleading in this regard). The throat is located approximately at the position shown in Figure 9, although this depends to some extent on the width of the exit slot. According to the theory the critical pressure ratio for sonic flow at the throat is $p_0/p_\infty \simeq 1{\cdot}53$, so the range of pressure ratios for which the Group A tones are generated is probably just above the critical value. When the pressure ratio is barely above the critical value the flow should be over-expanded and in conventional convergent–divergent nozzles, at any rate, shock waves appear in the divergent part of the nozzle or at the nozzle exit leading to a subsonic exit flow. There are no signs of shock waves or Mach waves in the corresponding schlieren photographs (not shown here); indeed there are no particularly distinctive features at all. Thus the appearance of the schlieren photographs is consistent with subsonic jet flow.

A typical example of a Group A discrete tone is presented in Figure 12(b). Spectra were obtained for the full range of observer angles. The directivity is not pronounced, but the intensity of the tone does diminish markedly for observer angles exceeding about 20° or 30° above the horizontal. This is consistent with the sound source being near the exit slot and the body of the Coanda model partially shielding observers located above the horizontal. The authors are unable to propose a convincing mechanism for the generation of these tones. The actual value of the frequency is around 20 kHz which is close to that of the discrete tones generated when a step is installed between the exit slot and the Coanda surface (see reference [24] and Part 2 of the present paper). However, this is probably a coincidence, since the mechanism identified for the generation of the tones when a step is present involves the base-flow region downstream of the step. It is certainly a coincidence that the dominant tone in Figure 12(b) is similar to the lower-frequency tone in Figure 12(c), since as remarked above these Group B tones are characterized by peak frequencies which fall sharply with a rise in pressure ratio.

In the absence of a convincing explanation it is natural to ask whether these Group A tones are actually facility noise rather than an aeroacoustic phenomenon. Whilst one would not claim to be able to eliminate this possibility entirely, it should be noted that for the present stepless Coanda model the tones only occurred for Slot B over a limited range of pressure ratios. It is true that discrete tones of roughly similar frequency were observed with stepped Coanda models (as described in Part 2), but in this case the

frequency varied in a consistent manner with step height in line with the theoretical model proposed in Part 2. This suggests that on the stepped model, at least, the tones were aeroacoustic in origin and not facility noise. Furthermore tones could be completely eliminated for all pressure ratios by using a saw-toothed exit slot as described in Part 2. Thus the balance of the evidence suggests that the Group A discrete tones, typified by the spectra in Figure 12(b), are aeroacoustic in origin rather than facility noise.

### 5.2. BROAD-BAND SHOCK-ASSOCIATED NOISE

Much is now known about shock-associated noise for round jets (see reference [38] and a recent review by Tam [39]) and there is a good theoretical model to explain many of its observed features (see references [40, 41]). Although the Coanda flow is far more complex than that of a round jet, owing to the effects of the solid surface and shock–shock and shock wave–boundary layer interactions, it is possible to derive an approximate model based on the approach of Tam *et al*., especially in the light of Tam's [42] extension of the theory to non-axisymmetric supersonic jets.

The theoretical model is based on the assumption that the coherent structures in the supersonic mixing layer that develops near the exit slot can be modelled as instability waves by using linear stability theory, so that the associated velocity perturbations take the form

$$u_w = \hat{u}_w \exp[\mathrm{i}(k_w x - \omega t)] + c.c. \tag{9}$$

where $k_w$ and $\omega$ are respectively the wave number and frequency of the coherent structure (or instability wave), $x$ is measured along the "undisturbed" free jet boundary starting at the slot exit, and $c.c.$ denotes the complex conjugate. The shock-cell structure of the underexpanded jet can be modelled by linearized supersonic jet theory and can be assumed to give rise to a velocity perturbation of the form

$$u_s = \sum_{j=1}^{\infty} \hat{u}_{sj} \underbrace{(\tfrac{1}{2}\,\mathrm{e}^{\mathrm{i}k_{sj}x} + \tfrac{1}{2}\,\mathrm{e}^{-\mathrm{i}k_{sj}x})}_{\cos(k_{sj}\,x)}, \tag{10}$$

where the $k_{sj}$ correspond to the successive eigenmodes of the shock-cell structure, $k_{s1}$ corresponding to the primary shock-cell wavelength.

The shock-cell structure can be considered as a sort of waveguide. The coherent structures (instability waves) interact with the shock-cell structure to produce disturbances of the form

$$(\hat{u}_w\,\hat{u}_{sj}/2)\exp[\mathrm{i}(k_w - k_{sj})x - \omega t]. \tag{11}$$

If $k_{sj}$ and $k_w$ are close in value the phase speed $c = \omega/(k_w - k_{sj})$ will be supersonic. Thus, in analogy with steady supersonic flow over a wavy wall, Mach waves are radiated downstream at an angle $\theta_{sa}$ given by

$$a_\infty/c = a_\infty\,(k_w - k_{sj})/\omega = \cos\theta_{sa}. \tag{12}$$

If it is assumed that the primary shock-cell wavelength is paramount, the frequency of the Mach wave radiation (the broadband shock-associated noise) is given by

$$f = U_c/\{L_s\,[1 - (U_c/a_\infty)\cos\theta_{sa}]\} \tag{13}$$

where $L_s = 2\pi/k_{s1}$ is the primary shock cell wavelength and $U_c = \omega/k_w$ is the phase speed of the instability wave (i.e., the convection speed of the coherent structure). Note that if

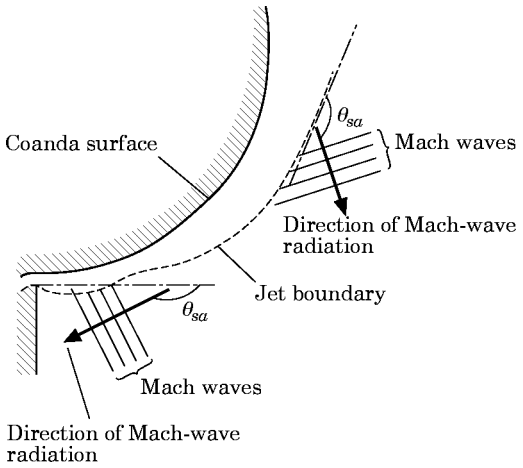


Figure 13. A schematic sketch depicting Mach-wave radiation.

$k_{s1} < k_w$ then $\theta_{sa} > \pi/2$ and $\cos\theta_{sa} < 0$, implying that the Mach waves radiate *upstream* towards the exit slot.

For the unforced mixing layer the coherent structures have a range of convection speeds $\Delta U_c$, say. It can be readily shown (see reference [41]) that equation (13) implies that the corresponding band of frequencies in the noise spectrum is given by

$$\Delta f \simeq (\mathrm{d}f/\mathrm{d}U_c)\Delta U_c = [1 - (U_c/a_\infty)\cos\theta_{sa}]^{-2}\Delta U_c/L_s. \tag{14}$$

The factor multiplying $\Delta U_c$ in equation (14) decreases in value rapidly as $\theta_{sa} \to \pi$. For a round jet this implies that the noise spectrum becomes much more narrowband as the direction of radiation approaches the nozzle outlet axis. This feature is indeed observed in the noise spectra from supersonic round jets. The peak also increases in amplitude.

Figure 13 depicts schematically the implications of applying the theoretical model of Tam *et al*. to the present supersonic Coanda flow. Two possibilities are depicted: Mach-wave radiation from (i) the mixing-layer region near the exit slot where the shock waves are strongest, and from (ii) the region in the vicinity of the maximum diameter, where the coherent structues are probably strongest (see the discussion in section 4.2). In this connection it should be noted that schlieren photographs (not presented here) show that the shock-cell pattern persists as far as the location of maximum diameter for relatively high values of $p_0/p_\infty$. In either case (i) or (ii) the directions in which shock-associated noise would be most dominant are oriented well below the horizon and would not be likely to be prominent over the range of observer angles for which measurements were taken. There is certainly no obvious sign of the noise spectra presented in reference [27] becoming more narrow-band as the observer angle, $\theta$, becomes increasingly negative. Accordingly, on the basis of present evidence, it may be concluded that broadband shock-associated noise is probably not an important noise source for supersonic Coanda flows in the usual range of observer directions.

### 5.3. A SCREECH MECHANISM FOR THE GROUP B DISCRETE TONES

For all slots except A discrete tones were observed at high values of $p_0/p_\infty$. The data available for the unstepped Coanda model are rather limited and are presented in Table 2.

The variation of the dominant (i.e., the most intense) frequency with $p_0/p_\infty$ is very similar to that found for the stepped Coanda model (see Figure 8 of Part 2). Much more data

TABLE 2

*Measured Group B discrete-tone frequencies*

| Exit-slot type | Slot width (mm) | $p_0/p_\infty$ | Frequency (kHz) |
|---|---|---|---|
| B | 1·25 | 6·52 | 18·3 |
| — | — | — | 22·2 |
| — | — | — | 41·3 |
| — | — | — | 60·1 |
| — | — | — | 64·3 |
| C | 1·875 | 5·14 | 18·0 |
| — | — | — | 35·3 |
| C | 1·875 | 6·52 | 9·1 |
| — | — | — | 23·8 |
| D | 2·5 | 5·14 | 6·7 |
| — | — | — | 13·9 |
| — | — | — | 20·6 |
| — | — | — | 27·6 |
| — | — | — | 42·2 |

on the discrete tones are available for the stepped Coanda models. In this case the dominant frequency drops steeply with a rise in pressure ratio for fixed step height and exit-slot width. Two theoretical models will be proposed and examined for the generation of the Group B discrete tones. The first is based on the model proposed by Tam *et al*. [41, 42] for jet screech. The second mechanism involves the dynamics of the separation bubbles and is described in section 5.4. Both theoretical models rely on a feedback loop being set up. The role of a feedback loop in generating jet screech was first proposed in the seminal papers of Powell [43, 44].

For conventional jets Tam *et al*. [41] noted that the frequency of jet screech appears to be close to the limit of the peak frequency of broadband shock-associated noise as the observer angle tends towards 180°. This led them to propose that the Mach-wave radiation described above plays a key role in the feedback loop for jet screech. They argued that the coherent structures (instability waves) near the end of the potential core, where they are most powerful, would generate intense Mach-wave radiation upstream towards the nozzle lip. Mach waves with $\theta_{sa} \simeq \pi$ would not only have the appropriate directivity but would also be the most intense and narrow-band. Upon reaching the nozzle lip these intense Mach waves would trigger instability waves which would travel downstream thereby closing the feedback loop.

For feedback loops the phase change occurring over the complete loop must equal $2n\pi$ (where $n$ is an integer). For most self-excited oscillation systems, for example edge and cavity tones, the feedback path length is fixed and controls the frequency generated (see the second mechanism proposed below in section 5.4 and that proposed in Part 2 for the Group A tones generated with a step present). On the other hand for the screech mechanism proposed by Tam *et al*. the above condition on the phase can be satisfied by slight changes in the feedback path effected by adjustments to the wave amplitude without imposing any condition on the oscillation frequency. Thus the screech frequency can be determined from equation (13) by setting $\theta_{sa} = \pi$. In this way an approximate way of estimating the screech frequency for the Coanda jet can be easily derived as follows. If it is assumed that for a particular value of $p_0/p_\infty$ (i.e., for fixed Mach number $M_j$ along the jet boundary near the nozzle exit) the convection

TABLE 3

*Theoretical screech frequency as a function of $p_0/p_\infty$ for slot C*

| $p_0/p_\infty$ | $M_j$ | $L_s/(L_s)_{2D}$ | $(f_s)_{2D}\,h/U_j$ | $f_s$ (kHz) | Observed frequency (kHz) |
|---|---|---|---|---|---|
| 2·72 | 1·29 | 0·624 | 0·226 | 13·8 | No discrete tones |
| 3·07 | 1·37 | 0·835 | 0·187 | 15·2 | No discrete tones |
| 3·41 | 1·45 | 0·900 | 0·158 | 14·4 | No discrete tones |
| 3·76 | 1·52 | 0·960 | 0·137 | 13·8 | No discrete tones |
| 4·45 | 1·63 | 0·965 | 0·113 | 12·0 | No discrete tones |
| 5·14 | 1·73 | 0·970 | 0·091 | 10·1 | 18·0 |
| — | — | — | — | — | 35·3 |
| 5·83 | 1·81 | 0·980 | 0·079 | 9·1 | No discrete tones |
| 6·52 | 1·88 | 0·990 | 0·07 | 8·4 | 9·1 |
| — | — | — | — | — | 23·8 |

speeds $U_c$ of the coherent structures (instability waves) for the Coanda and plane two-dimensional jets are more or less the same, then the screech frequencies of the two jets are simply related by

$$f_s \simeq \{L_s/(L_s)_{2D}\}(f_s)_{2D}. \tag{15}$$

It should be noted, that since the Coanda jet corresponds to only half of a conventional jet, the width, $h$, of the exit slot for a two-dimensional jet is equivalent to $2b$. $f_s\,h/U_j$, the non-dimensional screech frequency for a supersonic two-dimensional jet is plotted against $M_j$ in Figure 7 of Tam [42]. $L_s/(L_s)_{2D}$ can be estimated from method-of-characteristics calculations, like that illustrated in Figure 7, carried out for the supersonic two-dimensional and Coanda wall jets. $L_s/(L_s)_{2D}$ is then taken to be equal to the ratio of the distances from the nozzle exit to the first maximum of the jet-boundary displacement. In this way the estimates given in Table 3 were obtained.

It can be seen from Table 3 that the proposed screech mechanism does predict frequencies that are not too far removed from the lowest observed frequency in the case of $p_0/p_\infty = 6{\cdot}52$ at least. It also gives a drop in frequency with rising pressure ratio, although not so steep as found in the experimental observations for both stepped and unstepped Coanda models. The approximate theoretical model encapsulated in equation (15) would suggest that to a rough approximation $f \propto 1/b$. This is found to be roughly consistent with the experimental data presented in Table 2 for two pressure ratios and three exit-slot widths. What the screech model does not explain, if it involves the interaction of the shock-cell pattern and the coherent structures of near-exit-slot mixing-layer region, is why the Group B discrete tones are only seen at high pressure ratios. Another difficulty with the screech mechanism is that, as will be seen in Part 2 for a fixed value of exit-slot width, $b$, the tone frequencies vary in a very similar way with $p_0/p_\infty$ irrespective of whether or not there is a step between the exit slot and the Coanda surface. Yet the presence of such a step radically alters the shock-cell structure near the exit slot. This suggests that, if there is a screech mechanism operating, it must involve the coherent structures further downstream near the point of maximum diameter. The absence of discrete tones at lower values of $p_0/p_\infty$ could then be explained by the fact that it is only at relatively high values of $p_0/p_\infty$ that the shock-cell pattern extends to the position of maximum diameter. But, as is plain from Figure 13, the Mach-wave radiation generated by the interaction of the coherent structures in the vicinity of the maximum diameter and the shock-cell structure there does not appear to have an acoustic path back to the exit slot. Therefore, on balance, the proposed screech mechanism is not considered likely to be responsible for the Group B discrete tones.

### 5.4. A FEEDBACK MECHANISM INVOLVING SEPARATION-BUBBLE DYNAMICS

Separation bubbles were always present on the Coanda surface when the Group B tones were generated. Separation bubbles did not form for exit slot A (with the smallest exit-slot width) and no discrete tones were observed in this case. This motivated the authors to look for a feedback mechanism for tone generation which involves the dynamics of the separation bubbles.

Figure 14 depicts a theoretical model for a self-excited feedback mechanism which could possibly explain the generation of these tones. Essentially one postulates that strong wave-like disturbances are generated downstream of the separation shock-wave and grow along the separated boundary layer. When the disturbances reach the reattachment point they would cause periodic inflow and outflow from the separation bubble, thereby giving rise to an acoustic monopole source which would radiate sound upstream within the subsonic separated flow.

These wave-like disturbances would also cause the reattachment shock-wave (not shown in Figure 14) to oscillate, thereby giving rise to a strong oscillating force acting normal to the solid surface. This would produce a dipole source having a cosine-type directivity with the direction of maximum intensity perpendicular to the surface and the direction of zero intensity along the surface. Thus this type of acoustic source would not radiate intense sound waves back to the separation point to provide a return feedback path. However, if dipole sources with the appropriate directivity are associated with the unsteady separation-bubble dynamics, the approximate approach described below would still remain valid.

Suppose that the common frequency $f$ of the generated sound and disturbance satisfy the relationship

$$(1/c + 1/a)fL_B = n, \qquad n = 1, 2, 3, \ldots, \tag{16}$$

where $c$ is the phase speed of the disturbances, $a$ is the speed of sound in the separation bubble and $L_B$ is the length of the separation bubble. When equation (16) is satisfied the sound arrives at the leading edge of the separation bubble in phase with the disturbances, thereby establishing a self-excited feedback loop. Here the approach is based on the assumption that $L_B$ is more or less fixed. In reality $L_B$ would be adjustable to some extent, since it would be affected by the amplitude and phase of the disturbance. $L_B$ can

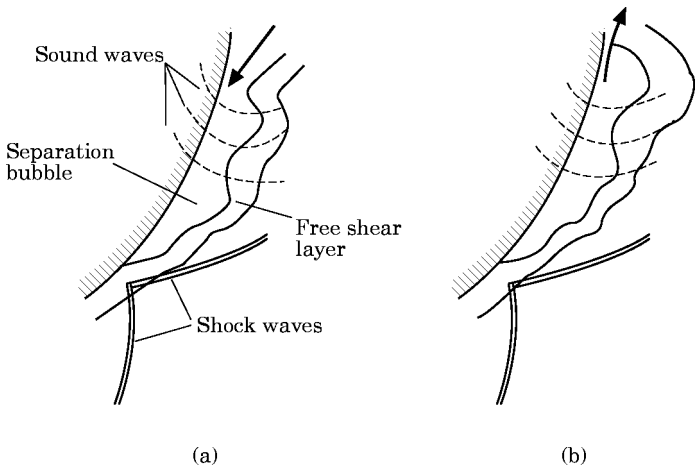


Figure 14. A schematic sketch of the theoretical model for the generation of discrete tones. (a) Inflow to bubble; (b) outflow from bubble.

TABLE 4

*Comparison of predicted and observed discrete tone frequencies*

| Slot | $p_0/p_\infty$ | $L_B$ (mm) | $n$ | Eq. 17 (kHz) | Observed frequency (kHz) |
|---|---|---|---|---|---|
| B | 6·52 | 11·8 | 2 | 21·3 | 18·3 |
| C | 5·14 | 14·1 | 2 | 17·5 | 18·0 |
| D | 5·14 | 17·4 | 1 | 7·1 | 6·7 |

be measured approximately from the appropriate schlieren photographs and $U$ and $a$ can be estimated from the isentropic flow relationship. To obtain a rough estimate of the expected frequency from equation (16) it will be rather arbitrarily assumed that $c = U/2$, so that the predicted frequency is given by

$$f = n/\{(2/U + 1/a)L_B\}. \tag{17}$$

Table 4 compares the predicted frequency with the (lowest) measured frequency of the discrete tones.

The correspondence between the predicted and observed frequenices is close enough to lend credence to the theoretical model outlined above. When a step is present between the nozzle exit and the Coanda surface tones are generated far more readily. In this case it was found in reference [24] (see also Part 2) that at relatively high pressures the frequency of the tones decreases steadily with rising $p_0/p_\infty$. Since $L_B$ increases as $p_0/p_\infty$ grows larger this is precisely what one would expect from equation (17). Two groups of such tones were observed in reference [24] and Part 2. One group at moderate to high pressures and the other exclusively at high pressure. These appear to correspond to $n = 1$ and $n = 2$ in equation (17). The transition between the $n = 1$ and $n = 2$ stages appears to depend on the size of the slot width.

## 6. CONCLUSIONS

The high-speed Coanda flow investigated in this paper is a supersonic, axisymmetric wall jet which develops from an initial flow regime just downstream of the exit slot, consisting of an outer mixing layer, a potential core, and a boundary layer on the Coanda surface. The wall jet displays some of the characteristics of its simpler, two-dimensional, low-speed counterparts, in particular, a tendency for the angle (measured around the Coanda surface from the exit slot) at which the flow separates to fall as the ratio of exit slot width to radius of curvature increases. However, as with other high-speed Coanda flows, it was observed that small changes in stagnation pressure can lead to a rapid reduction in this separation angle, probably owing to shock wave–boundary layer interaction producing a separation bubble on the Coanda surface.

The shock-wave system observed in the flow is highly complex, with wave systems present both inside the nozzle and in the jet flow at all supercritical operating conditions. It is believed that the internal shocks arise as a consequence of a change in the sign of the streamline curvature, and are likely to give rise to a separation bubble on the outer nozzle wall, leading to a more complex wave system than found in round jets.

The shocks generated within the nozzle reflect out into the jet where they interact with waves from two other sources. The first set of waves is caused by incorrect expansion since the flow is underexpanded under most operating conditions. The flow structures formed by these waves are analogous to the shock cells observed in round jets, and indeed there is a similar quasi-periodic structure of shocks and expansions in the Coanda flow. The

other mechanism responsible for the generation of waves is the radial expansion of the flow. This produces expansion waves which reflect from the jet boundary as compressions, slightly decelerating the flow ahead of the shock waves caused by underexpansion. The interaction of the boundary layer (wall layer in the fully developed wall jet) with shock waves from all three sources leads to the formation of separation bubbles on the Coanda surface, even at fairly modest operating pressures. The size of the bubble(s) is observed to grow with increasing operating pressure until the flow breaks away from the surface.

As to the acoustic characteristics of the high-speed Coanda flow, there is some evidence that, when discrete tones are absent from the *SPL* spectra, the *SPL* scales with $U^8$ and the square of the slot width. This is broadly consistent with the Lighthill theory, indicating that turbulent mixing noise is a major noise generation mechanism in this flow. But the spectral characteristics of the broadband noise do not appear to follow the expected scaling with slot width, and the limited evidence suggests a scaling with maximum diameter, indicating that the dominant noise generation region in the flow may be close to the point of maximum diameter.

Discrete tones are present in the *SPL* spectra at many high pressure operating conditions. Their presence appears to be linked to the large separation bubble, mentioned above, which forms on the Coanda surface and is caused by shock wave–boundary layer interaction. A simple mechanism to explain the generation of tones, based on a self-excited feedback loop, has been advanced, and this predicts tone frequencies which are in reasonably good agreement with the measured values.

Thus, although some of the gross aerodynamic and acoustic properties of the high-speed Coanda flow resemble those of more conventional supersonic jets, the details of the flow and noise generation mechanisms are highly complex, making such a flow a challenging test case for even the most sophisticated flow and acoustic prediction codes.

## ACKNOWLEDGMENTS

The work described in this paper was undertaken as part of a research programme supported by the SERC, BP Research Centre and Kaldair Ltd. Much of the work was carried out while Dr. Green was first an SERC CASE research studentship sponsored by BP Research Centre and later an SERC Research Fellow.

## REFERENCES

1. H. Coanda 1932 *Brevet Invent. Gr. Cl.* 2, *no.* 762688 *République Française*. Procédé de propulsion dans un fluide.
2. T. Young 1800 *Lecture to the Royal Society on* 16*th January*, 1800. Outlines of experiments and inquiries, respecting sound and light.
3. L. J. Pritchard 1957 *Journal of the Royal Aeronautical Society* **61**, 149–180. The dawn of aerodynamics.
4. R. Wille and H. Fernholz 1965 *Journal of Fluid Mechanics* **23**, 801–819. Report of the first European Mechanics Colloquium on the Coanda effect.
5. P. Bradshaw 1973 *AGARDograph* 169. Effects of streamline curvature on turbulent flow.
6. P. N. Green and P. W. Carpenter 1983 in *Proceedings of the* 3*rd International Conference on Numerical Methods in Laminar and Turbulent Flow*, *Seattle*, *USA* (C. Taylor, J. A. Johnson and W. R. Smith, editors), 104–112. Swansea: Pineridge Press. Method of integral relations for curved compressible mixing layers with lateral divergence.
7. J. Wilkins, R. E. Witheridge, D. H. Desty, J. T. M. Mason and N. Newby 1977 in *Proceedings of the Ninth Annual Offshore Technology Conference*, *Houston*, *USA*, 123–130. The design, development and performance of the Indair and Mardair flares.

8. D. H. Desty, J. C. Boden and R. E. Witheridge 1978 in *Proceedings of the* 85*th National Meeting of the American Institute of Chemical Engineering*, *Philadelphia*, *USA*. The origination, development and application of novel premixed flare burners employing the Coanda effect.
9. N. Fricker, R. H. Cullender, K. O'Brien and J. A. Sutton 1986 in *Proceedings of the International Gas Research Conference*, *Toronto*, *Canada* (T. L. Cramer, editor), 989–1003. Rockville MD: Government Institutes Inc. Coanda jet pumps—Facts and fallacies.
10. I. C. Cheeseman and A. R. Seed 1966 *Journal of the Royal Aeronautical Society* **71**, 451–467. The application of circulation control by blowing to helicopter rotors.
11. J. N. Nielsen (editor) 1987 *Proceedings of the Circulation Control Workshop* 1986, *NASA Conf. Pub*. 2432.
12. N. J. Wood and J. N. Nielsen 1986 *American Institute of Aeronautics and Astronautics*, *Journal of Aircraft* **23**, 865–875. Circulation control airfoils as applied to rotary-wing aircraft.
13. A. Zandieh and J. G. Leishman 1993 *American Institute of Aeronautics and Astronautics*, *Journal* **31**, 1769–1776. Boundary layer and pressure measurements on a cylinder with unsteady circulation control.
14. J. H. Nichols and M. J. Harris 1987 reference [11], 479–489. Fixed wing CCW aerodynamics with and without supplementary thrust deflection.
15. D. W. Riddle and J. C. Eppel 1987 reference [11], 539–567. A potential flight evaluation of an upper-surface-blowing/circulation-control-wing concept.
16. P. M. Bevilaqua and J. D. Lee 1987 reference [11], 289–312. Design of supersonic Coanda jet nozzles.
17. H. R. Velkoff and C. Tung 1991 *Proceedings of the Fourth Annual Forum of the American Helicopter Society*, *Phoenix*, *Arizona*, 1259–1274. Aerodynamic design of a Coanda induced force and thruster anti-torque system.
18. D. H. Desty 1983 *Proceedings of the Institution of Mechanical Engineers* **197A**, 159–170. No smoke with fire.
19. M. Ameri and A. Dybbs 1993 in *Proceedings of SPIE*, *Laser Anemometry Advances and Applications* **2052**, 289–296. Coanda ejector—Why it works.
20. M. Ameri and A. Dybbs 1993 in *American Society of Mechanical Engineers*, *Fluids Engineering Division*, *Fluid Machinery*—1993 **163,** 43–48. Theoretical modeling of Coanda ejectors.
21. B. G. Jenkins, F. D. Moles, D. H. Desty, J. C. Boden and G. Pratley 1980 *Energy Technology Conference and Exhibition*, *New Orleans*, *ASME Paper* 80-*Pet*-86. The aerodynamic modelling of flares.
22. P. W. Carpenter and P. N. Green 1983 *American Institute of Aeronautics and Astronautics Eigth Aeroacoustics Conference*, *Atlanta*, *Paper AIAA*-83-0758. Noise sources in external Coanda-type gas flares.
23. P. W. Carpenter and P. N. Green 1984 *Proceedings of the Institute of Acoustics* **6**, 195–201. The generation of noise in external Coanda-type waste-gas flares.
24. P. W. Carpenter, D. W. Bridson and P. N. Green 1986 *American Institute of Aeronautics and Astronautics* 10*th Aeroacoustics Conference*, *Seattle*, *Paper AIAA*-86-1865. Features of discrete tones generated by jet flows over Coanda surfaces.
25. P. Li and N. A. Halliwell 1985 *Journal of Sound and Vibration* **99**, 475–491. Industrial jet noise: Coanda nozzles.
26. M. Salikuddin, W. H. Brown and K. K. Ahuja 1987 *American Institute of Aeronautics and Astronautics*, *Journal of Aircraft* **24**, 55–64. Noise from a circulation control wing with upper surface blowing.
27. P. N. Green 1987 *Ph.D. Thesis*, *University of Exeter*, *U.K.* The fluid dynamics and aeroacoustics of external Coanda flares.
28. B. G. Newman 1962 in *Boundary Layer and Flow Control* **1** (G. V. Lachmann, editor), 232–264. Oxford: Pergamon Press. The deflexion of plane jets by adjacent boundaries—Coanda effect.
29. J. F. Morrison and D. G. Gregory-Smith 1984 *International Journal of Heat and Fluid Flow* **5**, 139–148. Calculation of an axisymmetric turbulent wall jet over a surface of convex curvature.
30. D. G. Gregory-Smith and M. J. Hawkins 1991 *International Journal of Heat and Fluid Flow* **4**, 323-330. The development of an axisymmetric curved turbulent wall jet.
31. I. N. Sokolova 1986 *Fluid Mechanics—Soviet Research* **15**, 1–6. Investigation of supersonic Coanda flow.
32. D. G. Gregory-Smith and A. R. Gilchrist 1987 *International Journal of Heat and Fluid Flow* **8**, 156–164. The compressible Coanda wall jet—an experimental study of jet structure and breakaway.

33. L. J. S. Bradbury and M. N. Wood 1965 *Royal Aircraft Establishment*, *Technical Report No*. 65235. An exploratory investigation into the deflection of the thick jets by the Coanda effect.
34. A. R. Gilchrist and D. G. Gregory-Smith 1988 *International Journal of Heat and Fluid Flow* **9**, 286–295. Compressible Coanda wall jet: predictions of jet structure and comparison with experiment.
35. M. J. Lighthill 1952/54 *Proceedings of the Royal Society* **211A**, 564–587 and **222A**, 1–32. On sound generated aerodynamically.
36. C. Parsons 1988 *Ph.D. Thesis*, *University of Exeter*, *U.K.* An experimental and theoretical study of the aeroacoustics of external-Coanda flares.
37. C. Smith and P. W. Carpenter 1995 *Journal of Sound and Vibration* **185**, 397–413. The effect of solid surfaces on turbulent jet noise.
38. J. M. Seiner 1984 *American Institute of Aeronautics and Astronautics Ninth Aeroacoustics Conference*, *Williamsburg*, *Virginia*, *Paper AIAA*-84-2275. Advances in high speed aeroacoustics.
39. C. K. W. Tam 1995 *Annual Review of Fluid Mechanics* **27**, 17–43. Supersonic jet noise.
40. C. K. W. Tam and H. K. Tanna 1982 *Journal of Sound and Vibration* **81**, 337–358. Shock-associated noise of supersonic jets from convergent-divergent nozzles.
41. C. K. W. Tam, J. M. Seiner and J. C. Yu 1986 *Journal of Sound and Vibration* **110**, 309–321. Proposed relationship between broadband shock associated noise and screech tones.
42. C. K. W. Tam 1988 *Journal of Sound and Vibration* **121**, 135–147. The shock-cell structures and screech tone frequencies of rectangular and non-axisymmetric supersonic jets.
43. A. Powell 1953 *Journal of the Acoustical Society of America* **25**, 385–389. The noise of choked jets.
44. A. Powell 1953 *Aeronautical Quarterly* **4**, 103–122. On the noise emanating from a two-dimensional jet above the critical pressure.